

The boiling crisis of water under exponentially escalating heat inputs in subcooled flow boiling at atmospheric pressure

A. Kossolapov^a, F. Chavagnat^a, R. Nop^{a,b,c}, N. Dorville^c, B. Phillips^a, J. Buongiorno^a, M. Bucci^{a,*}

^aDepartment of Nuclear Science and Engineering, Massachusetts Institute of Technology, Cambridge MA 02138, USA

^bUniversité Paris-Saclay, CNRS, LIMS, 91400, Orsay, France.

^cUniversité Paris-Saclay, CEA, Service de thermo-hydraulique et de mécanique des fluides, 91191, Gif-sur-Yvette, France.

* corresponding author: mbucci@mit.edu

ABSTRACT

We investigated the boiling crisis of water under exponentially escalating heat inputs using a specially-designed experimental apparatus featuring high-speed infrared thermography to measure the time-dependent temperature and heat flux distributions on the boiling surface, and high-speed video diagnostics to image the bubble growth process. We conducted flow boiling experiments with water at atmospheric pressure on a plate-type heater installed in a $3 \times 1 \text{ cm}^2$ cross section channel. We tested various values of flow velocity (corresponding to Reynolds numbers from 0 to 35000), water subcooling (from 10 to 75 °C) and rate of power rise (corresponding to exponential power escalation periods, τ , from 1.5 to 500 ms). At long periods critical heat flux (CHF) is independent of the power escalation period and the boiling processes appear to be physically similar to steady state. As the period decreases, the CHF values tend to increase following an asymptotic $1/\sqrt{\tau}$ trend. The mechanism that determines this trend depends on subcooling. For high subcooling, CHF monotonically increases as the period decreases, and the DNB occurs through a fully developed nucleate boiling process. By contrast, for low subcooling, CHF first increases as observed for high subcoolings, then decreases, and finally increases again as the period decreases. We observe that such non-monotonic transition is due to a change in the boiling crisis mechanism. Specifically, for very short periods and low subcooling, the boiling crisis happens during the growth of the very first generation of bubbles, which never detach from the heated surface, shortly after the onset of nucleate boiling. In such cases, fully-developed boiling is not achieved.

Keywords

Transient flow boiling crisis

Exponential power escalation

Critical heat flux

1. Introduction

Reactivity initiated accidents (RIAs) form a group of design basis accidents (DBA) in nuclear reactors safety analysis. They are caused by a rapid insertion of reactivity, e.g., due to an unanticipated extraction of control rods, which may bring the reactor into a super prompt-critical state. This causes the reactor power \dot{Q} to rise exponentially as $e^{t/\tau}$ where the power escalation period τ depends on the value of the reactivity step and the nuclear characteristics of the reactor fuel. For large reactivity insertions the period τ could be as short as a few milliseconds. The occurrence of such transients poses a potential threat to the fuel integrity. Mitigation of RIAs is achieved through the reactivity feedback. In commercial light water reactors (LWRs) where the fuel Doppler effect dominates, the reactor returns to a stable state as soon as the fuel temperature becomes sufficiently high. However, the outcome may be different for research pool type reactors where highly enriched fuel is often used. In such reactors the Doppler effect is less important, and the void formation is the most important reactivity feedback. The lack of the Doppler effect allows the reactor power to raise unhindered until sufficient amount of void (i.e., steam) is created due to boiling. However, such time lag

could lead to high heat fluxes on the cladding surface, sufficient to cause the departure from nucleate boiling (DNB). The transition to film boiling can lead to fuel meltdown and failure of the cladding. If so, the molten fuel could be expelled, fragmented and lead to steam explosion. Therefore, in order to improve the accuracy of reactor safety analyses for such accidents, it is important to understand the physical mechanisms that lead to DNB, as well as to quantify the value of the critical heat flux (CHF) for which this phenomenon occurs.

Transient boiling heat transfer has been an active research topic since the beginning of the nuclear industry. Several integral effect test programs, such as BORAX [1], SPERT [2,3], NSRR [4] and CABRI [5] were carried out in order to understand the behavior of complex large scale systems under RIA conditions. These experiments demonstrated the need for better understanding of transient thermal-hydraulics phenomena. Recently, large scale out-of-pile experiments have been built to investigate DNB and post-DNB heat transfer [6], as well as the propagation of void between subchannels [7]. Requirement for better understanding of transient boiling heat transfer mechanisms has led to a number of small-scale experiments with carefully controlled operating conditions. Such studies were performed with a variety of fluids, at different system pressures and liquid subcooling. Our work focus on exponential power escalations at atmospheric pressure. Previous studies addressing similar operating conditions are summarized in Table 1. Note that other types of transients, such as power ramps and steps and temperature ramps are not considered here. The reader interested in those transient conditions is directed to Refs. [8] and [9].

Focusing on atmospheric pressure conditions (i.e., ~ 100 kPa), the key parameters influencing CHF under exponentially escalating heat inputs are liquid subcooling, mass flux or flow velocity, and power escalation period.

In steady state, higher subcooling always results in higher CHF. This same trend was observed in exponential transients by Rosenthal and Miller from 0 to 68 °C of subcooling (e.g., see Fig.13 in Ref. [10]), and Sakurai from 0 to 40 °C of subcooling (e.g., compare data for non-pre-pressurized water in Figs. 38 and 43 of Ref. [11]). However, Johnson's data for 5 ms period and low flow velocity (~ 0.3 m/s) surprisingly contradict this trend (see Tab.2 in Ref. [12]), as the CHF value does not change when the subcooling degree increases from ~ 23 °C to 62 °C (i.e., from 42 °F to 112 °F).

Little is known about flow effects, particularly at atmospheric pressure. Kataoka performed a few experiments on a wire heater at 0.143 MPa (i.e., close to atmospheric pressure). His results confirmed that CHF monotonically increases between 20 and 30 °C of subcooling and with the flow velocity, at all periods (e.g., see Fig.11 in Ref. [13]). However, there is a lack of data and understanding about flow effects at atmospheric pressure and particularly at high subcooling.

The effect of power escalation period τ is the least understood, and arguably the most intriguing. Most researchers observed that the CHF increases monotonically as the period is shortened [10-15]. However, Johnson's data show that, in low velocity flows, there is no change in the CHF value for highly subcooled conditions (with a 62 °C subcooling) when the period increases from 5 to 50 ms. Interestingly, Sakurai et al. [14] and Park et al. [15] observed that, in saturated conditions, the pool boiling CHF increases, decreases and increases again as the period decreases. However, this trend is less clear in subcooled conditions (e.g., see data for 40 °C of subcooling in Fig. 43 of Ref. [11]).

Based on his observations, Sakurai [11] proposed two distinct mechanisms of transient DNB, resulting in two different correlations. He argued that, for long periods and low subcooling (e.g., for periods higher than 100 ms in saturated pool boiling of water at ambient pressure), DNB is caused by hydrodynamic instabilities (HIs) and that, under such conditions, these instabilities are delayed as the period decreases, leading to higher CHF values. Instead, for short periods and low subcooling (e.g., for periods smaller than 100 ms in saturated pool boiling of water at ambient pressure), he argued that DNB occurs due to heterogeneous spontaneous nucleation (HSN) inside flooded cavities. However, the reasons for the non-monotonic CHF vs. period trend at low subcooling remain unclear.

A mechanistic model to predict transient CHF was developed by Serizawa [16] by modifying the model originally proposed by Haramura and Katto [17] for the steady state conditions. The latter assumes the presence of a thin liquid layer in contact with the heated surface (referred to as the "macrolayer"), underneath a large vapor clot. The macrolayer has vapor stems fed by the

evaporation of the liquid in contact with the surface. In turn, the vapor stems feed the vapor clot, which grows and eventually departs from the surface. When that happens, vapor stems merge to form a new clot and a new macrolayer. CHF is postulated to occur whenever the macrolayer is fully evaporated before the vapor clot can detach from the heated surface. Serizawa adapted this model to transient conditions. He applied an energy balance to the macrolayer in order to calculate the time of complete evaporation, by accounting for the time-dependent nature of the heat flux and introducing a macrolayer liquid supply term. However, to be able to fit the experimental data, the model required the empirical tuning of physical parameters, e.g., the initial macrolayer thickness. Later, Pasamehmetoglu [18,19] overcame this limitation by adopting a more mechanistic description of the macrolayer dynamics. However, as remarked by these authors [16,18,19], the physical description of macrolayer-based models is only suitable for relatively long power escalation periods and does not explain the trend observed as the period decreases further (i.e., the CHF decreases and then increases again).

Table 1. Overview of experimental studies on transient boiling CHF of water under exponentially escalating power inputs at (or close to) atmospheric pressure.

Study	Heater type	Diagnostics	Pressure [MPa]	Forced Flow [m/s]	Subcooling [°C]	Period [ms]
Rosenthal and Miller (1957) [10]	Vertical ribbon 2.54 mm wide 25.4 μm thick	<ul style="list-style-type: none"> High speed video (6000 fps); Resistance-based average temperature measurement 	0.1	None	0-68	5-75
Johnson (1971) [12]	Vertical ribbon 102 μm thick	<ul style="list-style-type: none"> High speed video; X-ray tomography; Resistance-based average temperature measurement 	0.1	≤ 0.30	5.6, 23, 62	5-50
Sakurai and Shiotsu (1977) [14]	Horizontal wire D = 1.2 mm	<ul style="list-style-type: none"> Resistance-based average temperature measurement 	0.1	None	0	5-5000
Kataoka et al. (1983) [13]	Vertical wire D = 0.8-1.5 mm	<ul style="list-style-type: none"> Resistance-based average temperature measurement 	0.143	1.35-4.04	20, 30	5-10000
Sakurai (2000) [11]	Horizontal wire D = 1.2 mm	<ul style="list-style-type: none"> High speed video (200 fps) Resistance-based average temperature measurement 	0.1	None	0, 40	5-20000
Park et al. (2009) [15]	Horizontal wire D = 1.0 mm	<ul style="list-style-type: none"> Resistance-based average temperature measurement 	0.1	None	0	5-20000
Present study	Vertical plate (see Sec. 2.1)	<ul style="list-style-type: none"> High speed video (20,000 fps) Infrared thermometry (2,500/12,000 fps) 	0.1	0 – 2.08	10, 25, 50, 75	1.5-500

In the studies performed in the previous decades, with limitations in the available diagnostics, only the average temperatures and heat fluxes on the surface of cylindrical or ribbon heaters could be quantified. In some cases, such information was supplemented with photographic data. However, the complex interaction between bubbles often obscures the images making it difficult to achieve a clear understanding of the physics governing the transient boiling process. Therefore, the hypotheses of Sakurai [11], Haramura and Katto [17], Serizawa [16] and Pasamehmetoglu et al. [19] could neither be proved nor disproved due to the lack of clear experimental evidences.

Recently, an investigation of transient boiling heat transfer was performed by our group [20,21]. The study provided a detailed characterization of single-phase heat transfer, ONB and fully developed nucleate boiling (FDNB) in exponential power escalations on a flat type heater, in both pool and flow boiling conditions. A wide range of water subcooling was explored at ambient pressures, representative of RIA scenarios in research pool type reactors with plate-type fuel elements. High temporal and spatial resolution diagnostics, i.e., high speed infrared and high-speed video cameras, were used to measure the time-dependent temperature and heat flux distributions on the boiling surface and to visualize the boiling process. The work improved the understanding of transient boiling, demonstrating the need of high-resolution diagnostics to clarify inconsistencies and contradictions in existing databases. The current work builds upon and extends that previous study to the boiling crisis. Precisely, it aims at shedding light on the physical mechanisms that lead to DNB in exponential power escalations, as well as at clarifying and quantifying the dependence of the CHF on power escalation period, subcooling, and mass flux, in water at atmospheric pressure.

2. Experimental apparatus and procedures

Experiments were run on the same apparatus as the one used in Ref. [22], with exception of a few modifications needed for transient tests. Figure 1 illustrates the experimental setup. Measurements were performed on a vertical flat heater in upward flow conditions. A high-speed infrared (HSIR) camera was installed behind the heater, to capture the infrared radiation emitted by the boiling surface. Two different HSIR cameras were used in the experiments. For relatively slow transients, we used an IRC806, which enabled a temporal resolution of 2,500 frames per second (fps) and spatial resolution of 115 $\mu\text{m}/\text{pixel}$. For fast transients, we used a Telops FAST M3k, which enabled a temporal resolution of 12,000 frames per second (fps) and spatial resolution of 65 $\mu\text{m}/\text{pixel}$. A Phantom v.12.1 high-speed video (HSV) camera was installed in front of the heater and used to image the bubbles on the boiling surface. High-speed videos were acquired with the temporal resolution of 20,000 fps and spatial resolution of 25 $\mu\text{m}/\text{pixel}$. Voltage and current were measured with Agilent U2542A high speed data acquisition system (HSDAS). An electrical shunt with a 1.67 m Ω resistance was used for current measurements. Two Chroma 62050P-100-100 DC power supplies were connected in series: they were used to amplify the exponential curve generated by the Rigol DG1022U function generator FG-2. The exponential curve was provided to the function generator in a form of a table containing 4095 discrete steps. The function generator then reproduced the table and sent a voltage signal to the power supplies. An amplification factor of 20 was applied to this signal by the power supplies. The amplified signal was then sent to the IR heater. The recordings of voltage and current through the heater were checked after each CHF test in order to confirm that the correct period of the exponential power input was achieved. Another function generator, FG-1, was used to provide a 5 V synchronization signal. At the beginning of each test, HSIR camera, HSDAS, FG-1 and FG-2 were initiated simultaneously by a 5 V triggering signal. Further, a controlled delay was introduced between the trigger and outputs of FG-1 and FG-2 to capture the beginning of the transient.

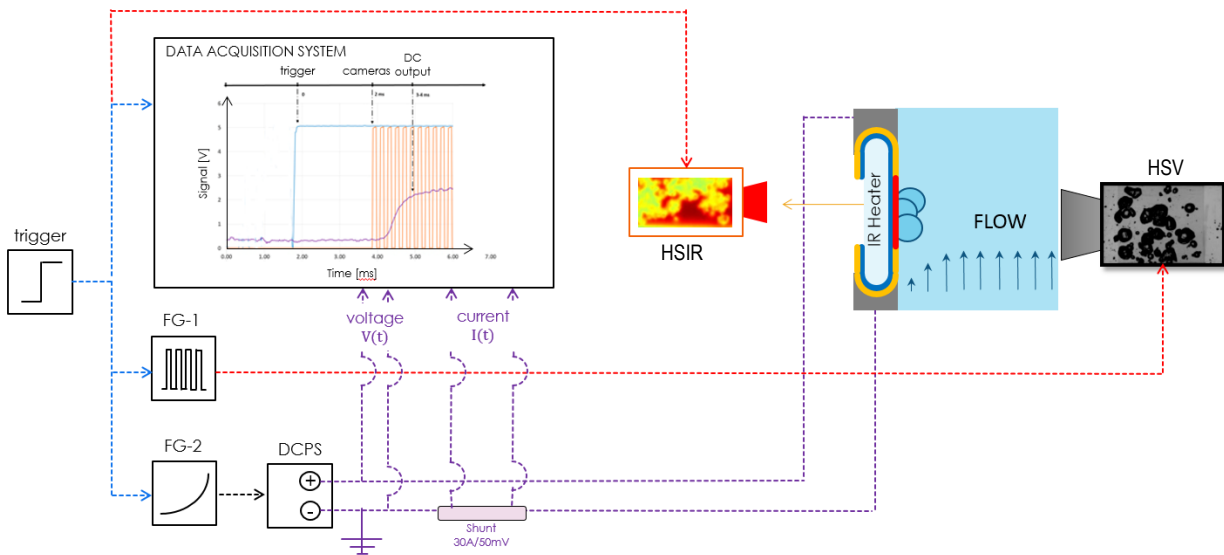


Figure 1. Schematic diagram of the experimental setup.

2.1. Infrared heater

Figure 2 shows the heater design. It consists of a 20x20 mm² sapphire substrate, 1 mm thick. An indium tin oxide (ITO) coating is wrapped around the substrate and serves as the Joule heater. The ITO coating is opaque in the 3-5 μm wavelength range and transparent in the visible light wavelengths. Sapphire instead is quasi-transparent in the 3-5 μm wavelength range. Such heater configuration allows an IR camera to record the 3-5 μm radiation emitted by ITO, while simultaneously allowing a high-speed video camera to image the heater from the front with an LED back-lighting (see Figure 1). The ITO is locally nano-smooth, with a thickness of 0.7 μm and a typical sheet resistivity of 2.5 Ω per square at ambient temperature. It is noteworthy that the relative change of the ITO resistivity with temperature, i.e., $\sim 80 \text{ pcm}/^\circ\text{C}$, is practically negligible within the temperature range covered by this investigation. This guarantees that the Joule heating is uniform over the ITO surface. Silver pads are deposited on top of the ITO and wrapped around the filleted edges of the sapphire substrate (see Figure 2). They define a square active ITO area of 10x10 mm² and allow a uniform supply of electric power to the heater surface.

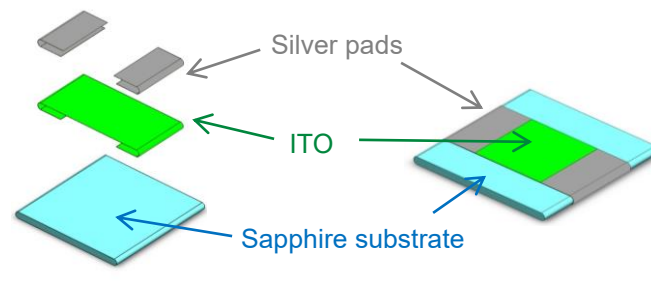


Figure 2. Exploded (left) and assembled (right) views of the IR heater.

2.2. Test section

Figure 3 shows the test section, which is made of 316 stainless steel. It has three openings to accommodate quartz windows and one opening for the installation of the heater cartridge. Both windows and the heater cartridge are held in place by stainless steel flanges. The test section is designed to operate at pressures up to 1.0 MPa and temperatures up to 180 $^\circ\text{C}$. The flow channel has a rectangular shape (3x1 cm²) with a hydraulic diameter of 1.5 cm. The entrance channel has the same cross section as the test section. The length of the entrance channel is 965 mm, i.e. roughly 65 hydraulic diameters, which ensures a fully-developed momentum boundary layer before the test section. The heater cartridge is used to provide a structural support for the IR heater, insulate it from the test section body and facilitate the electrical connections. The body of the cartridge is made of Shapal[®]. Copper

or Aluminum leads are connected from behind and are used to supply electrical power to the heater. The test section and the entrance region are connected to the flow loop which is equipped with a variable frequency pump, a flow meter, the temperature and pressure instrumentation, a preheater, a chiller, an accumulator, and filtering and degassing systems.

2.3. Calibration of the infrared camera

A brief description of the IR calibration technique is presented below. For more details about the technique and its validation, the reader is invited to consult Ref. [23]. The ITO emits IR radiation proportional to its temperature. However, in addition to the IR radiation from ITO, the IR camera also receives the radiation from the sapphire substrate (which is not completely transparent in the 3-5 μm wavelength range and whose optical properties are strongly wavelength dependent) and the radiation reflected from the background. Therefore, it is important to exclude contributions from the sapphire and background radiation from the total signal in order to measure the actual ITO temperature. This is achieved by solving an inverse problem coupling radiation and conduction. The problem is inverse because the boundary condition of the problem, i.e. the actual ITO temperature, is not known but is part of the solution, which is obtained iteratively. A guess ITO temperature is used as tentative boundary condition for the 3D conduction equation, which is solved in the sapphire substrate. The updated temperature distribution in the substrate is used to calculate the radiation emitted and reflected by the whole heater and received by the camera. This radiation is compared to the actual radiation detected by the IR camera. If these two radiation signals are not exactly the same, the guess ITO temperature is updated and the process is repeated until satisfactory convergence is achieved. Such procedure is applied to each IR frame throughout the transient. Importantly, the IR calibration technique also identifies the amount of heat absorbed by the sapphire substrate, $q''_s(x, y, t)$. The amount of heat absorbed by the substrate is subtracted from the total power generated in the ITO film, q'' , in order to calculate the amount of heat delivered to water, $q''_w(x, y, t)$. Knowing the heat absorption of the substrate is crucially important for the short period tests, for which the substrate can absorb a significant fraction of the total heat flux generated in the ITO film. This IR calibration technique has been extensively validated and used in many boiling experiment involving the same heater design (e.g., see Refs. [20–22, 24–26]).

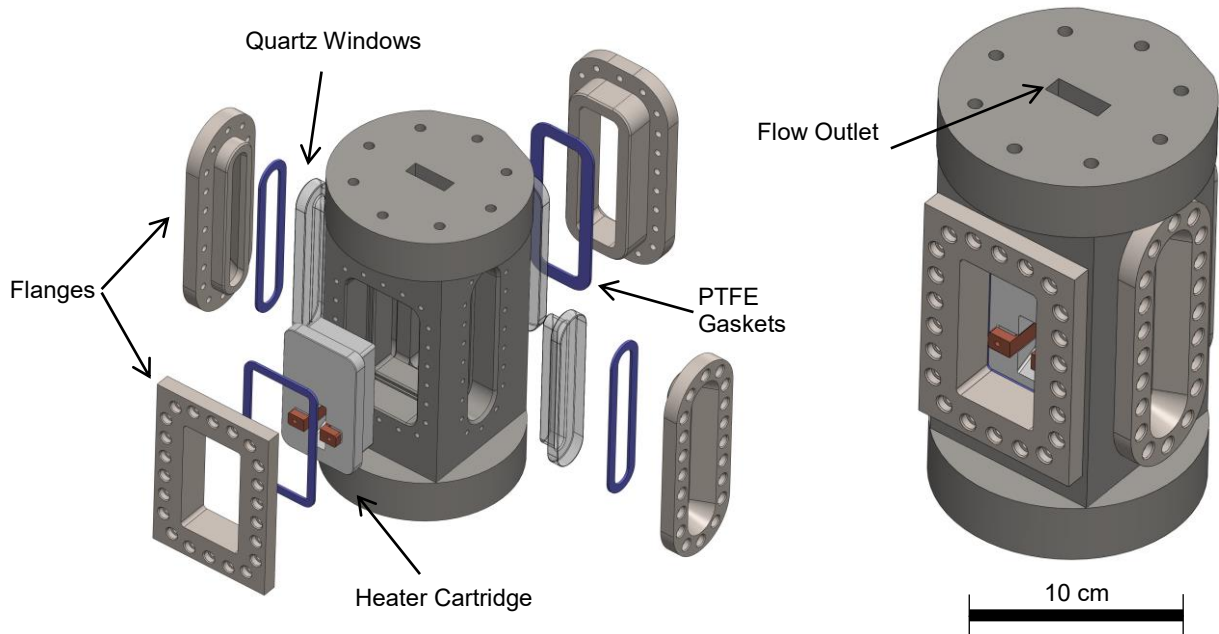


Figure 3. Test section design. Exploded (left) and assembled (right) views.

2.4. Experimental procedures and test matrix

Before each test the heater surface is degassed by inducing steady-state boiling for 30 minutes. This is assumed to remove non-condensable gases from the heater cavities. During the test, exponential power inputs with the same period but different peak values

were tested in sequence. The peak value was carefully increased until the appearance of an irreversible dry spot was observed. The power coast-down was executed as fast as possible to minimize the integral energy release during the power peak and reduce the risk of heater failure. The experimental conditions explored in the current work are summarized in Table 2.

Table 2. Operating conditions.

Parameter	Range			
Power escalation periods [ms]	1.5, 2.5, 3.5, 5, 7, 10, 20, 50, 100, 200, 500			
Subcooling [°C]	10	25	50	75
Reynolds number $\times 10^{-3}$ (Velocity [m/s]) (Mass Flux [kg/m ² /s])	16* (0.35) (338)	13.5* (0.35) (341)	8.5 (0.31) (306)	0.0** (0.0) (0)
	25* (0.54) (521)	25* (0.65) (634)	25 (0.92) (909)	25 (1.49) (1485)
	35 (0.76) (733)	35 (0.90) (877)	35 (1.29) (1274)	35 (2.08) (2073)
* 5 and 500 ms only ** 1.5, 2.5, 3.5, 5 and 500 ms only				

For the cases of 10, 25 and 50 °C of subcooling, the lowest values of Reynolds number were dictated by the lowest speed of the circulation pump. Presence of flow in the loop was necessary for maintaining constant bulk liquid subcooling throughout the test. For the cases of 75 °C subcooling the bulk temperature was almost identical to the room temperature. Therefore, the pump was turned off and experiments were performed in the stagnant liquid while still maintaining 75 °C of subcooling.

2.5. Detection of the boiling crisis and CHF measurements

It is challenging to clearly define CHF for transient boiling. In our experiments we defined CHF as the value of heat flux that creates the first irreversible dry spot on the boiling surface. An irreversible dry spot is such that it never gets rewetted once it appears on the boiling surface until the applied heat flux is eventually decreased. Generally, there is no stable state for such a dry spot; it can only grow, if the heat flux keeps growing, or shrink and be quenched, if the heat flux decreases. Figure 4 illustrates this process. It shows the time-dependent heat flux distributions of a test, starting from the appearance of the first few bubbles (0.0 ms) and ending with the whole heater surface covered by the vapor film. A dry spot is clearly seen on the second snapshot (16.0 ms), i.e. the extended area where the heat flux is essentially zero. However, this dry spot is eventually quenched (21.2 ms), so we classify this as a reversible dry spot. While the quenching proceeds, two new dry spots are formed on the top and the bottom of the heater (21.2 ms). These dry spots are irreversible because they continue to grow (22.8 ms). Eventually they coalesce (25.2 ms) and a combined dry spot continues to grow until a vapor film covers the whole heater area (47.6 ms).

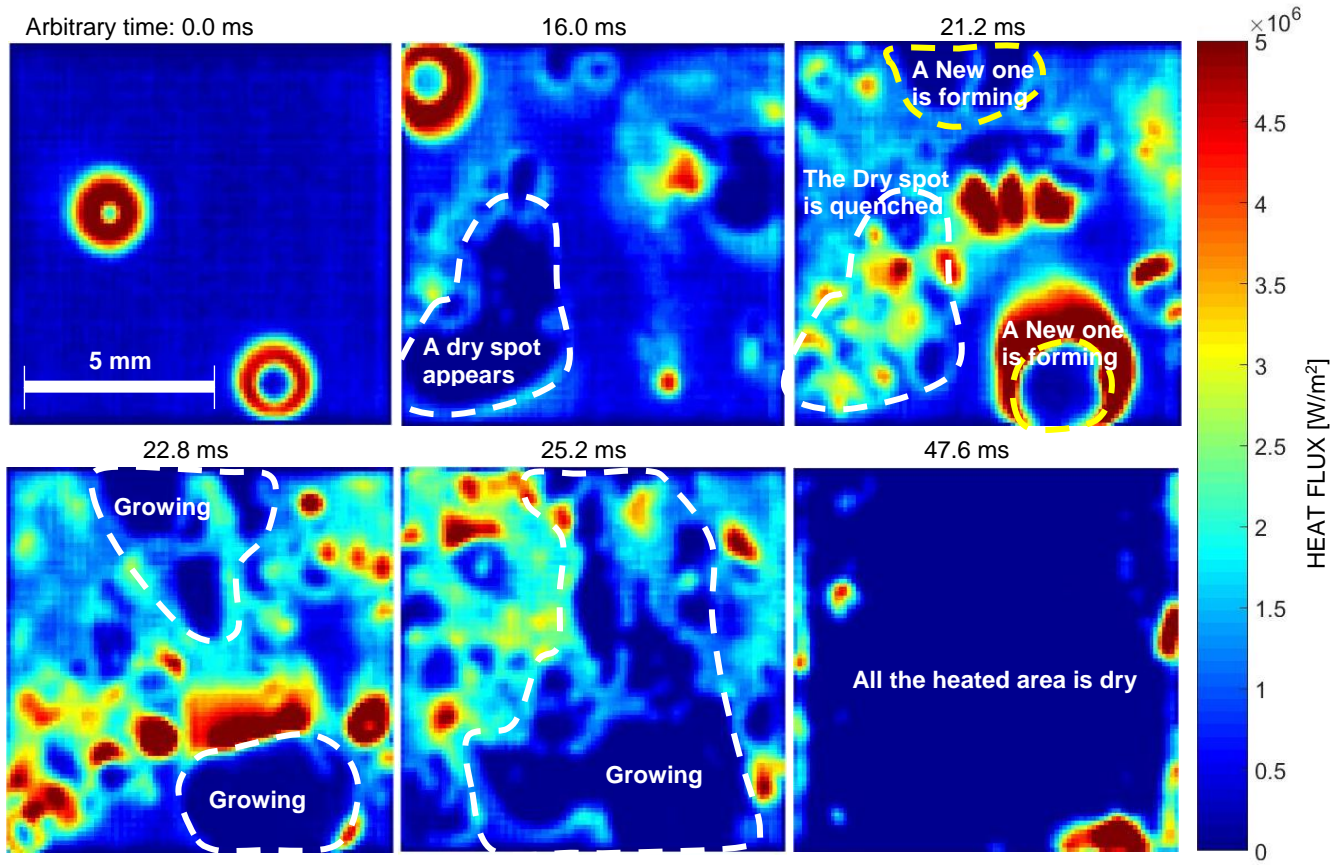


Figure 4. The heat flux distribution on the boiling surface reveals the escalation to CHF in the test at 10 °C of subcooling, 16000 Reynolds number and 50 ms power escalation period.

2.6. Measurement uncertainties

The absolute uncertainty of the CHF values $\Delta q''_{CHF}$ is given by three terms:

$$\Delta q''_{CHF} = \sqrt{(\Delta q''_m)^2 + (\Delta q''_t)^2 + (\sigma_{CHF})^2} \quad (1)$$

Here, $\Delta q''_m$ is the absolute measurement uncertainty related to the Joule heating, q'' , which is given by

$$q'' = \frac{I \cdot U}{A_H} \quad (2)$$

where I is the current, U is the voltage drop across the heater and A_H is the heater area. The absolute measurement uncertainty includes uncertainties of voltage ΔV and current ΔI readings:

$$\frac{\Delta q''_m}{q''} = \sqrt{\left(\frac{\Delta V}{V}\right)^2 + \left(\frac{\Delta I}{I}\right)^2} \quad (3)$$

Note that here the uncertainty of the heater area was omitted because it was much smaller than uncertainties of current and voltage readings. The measurement uncertainty for all tests was in the order of 0.1 MW/m².

$\Delta q''_t$ is the absolute temporal uncertainty related to the temporal resolution, i.e., the frame rate, of the IR camera. The occurrence of CHF was determined through the analysis of IR videos. Therefore, the temporal uncertainty associated with the identification of CHF is the inverse of the camera frame rate, i.e. $\delta t = 0.4$ ms for IRC806 or $\delta t = 83$ μ s for Telops FAST M3k. At short periods the heat flux could increase significantly over this period of time. Therefore, a conservative estimate of the temporal uncertainty of the CHF value is given by:

$$\Delta q_t'' = q_0'' \cdot [e^{t_{CHF}/\tau} - e^{(t_{CHF}-\delta t)/\tau}] \quad (4)$$

where q_0'' is the Joule heating heat flux at the beginning of the transient and t_{CHF} is the time when CHF happens. For short periods and high subcooling this term could be as large as 2 MW/m².

Lastly, for each operating condition the experiment was repeated three times, and σ_{CHF} is the standard deviation of the three measured CHF values.

For all measurements the temporal uncertainty typically dominates at short periods whereas the standard deviation is the biggest contributor to the uncertainty at the longer periods. In each figure presented next, values of the absolute CHF uncertainty are represented by error bars.

221

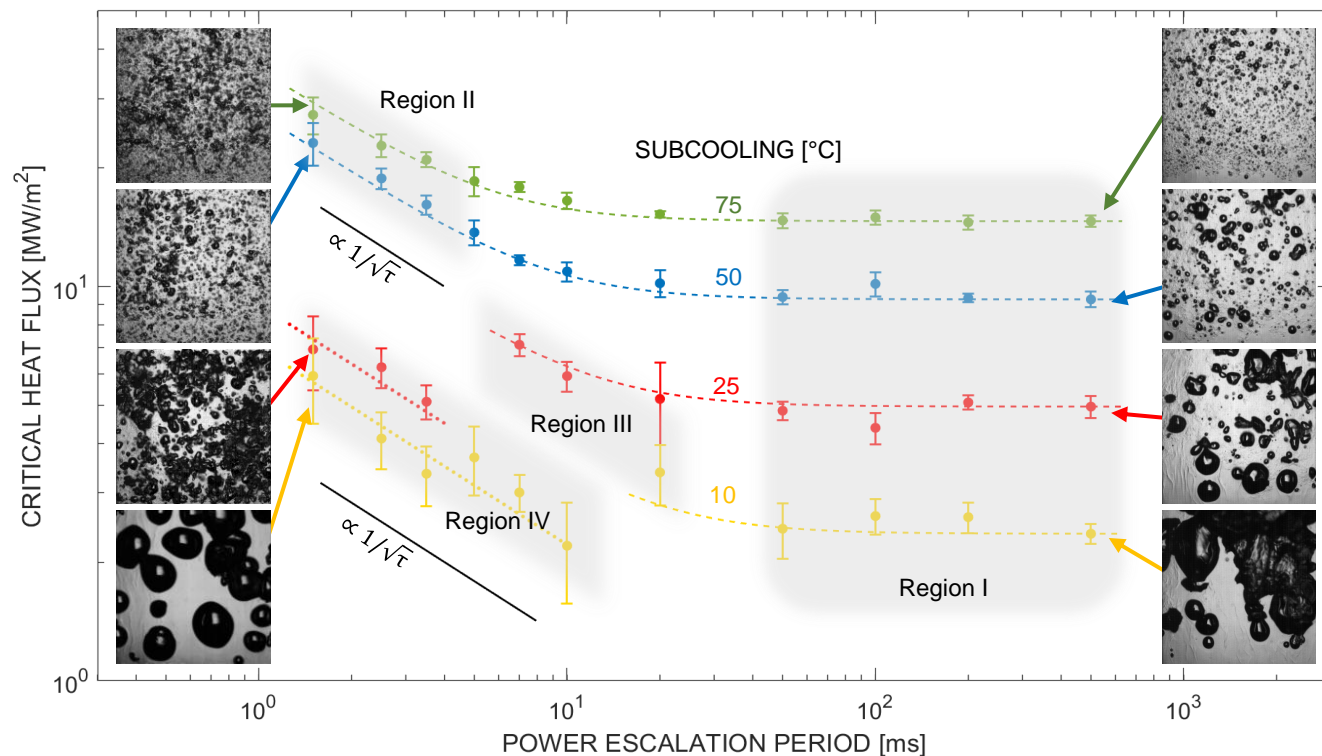
3. Results and discussions

222

223

224

Four macroscopic behaviors emerge from qualitative and quantitative observations of the boiling process and the boiling crisis. For a given flow rate, their classification is based on power escalation period and subcooling. They are identified in Figure 5, based on CHF values measured for tests with a Reynolds number of 35000.



225

226

227

228

229

Figure 5. CHF values vs. power escalation periods for tests run with a Reynolds number of 35000, at different subcooling degrees. The insets show images of the boiling surface (1×1 cm²) during the power escalation. Right images refer to tests with a 200 ms period, at 50% of the CHF value, whereas left images show the boiling surface shortly after the onset of nucleate boiling in the tests run with a period of 5 ms.

230

231

232

233

234

235

236

237

For given period, the CHF always increases with increasing subcooling, as expected. For slow transients, i.e., long periods (Region I), the CHF values do not depend on the power escalation periods. This finding suggests that the flow plays a dominant role in the bubble dynamics, and that the boiling process is similar to what can be expected for steady power inputs. For short periods and high subcooling, i.e., Region II, CHF always increases with decreasing period. Such trend is maintained even in the case of lower subcooling (Region III), if the period is not too short. The CHF increases also for very short periods (Region IV). However, between Region III and IV, as the periods decreases, there is a clear drop in the CHF values. Similarly, there seems to be a discontinuity between Region II and IV, when subcooling decreases for very short periods. The differences among these boiling regions and their transition are discussed hereafter.

238

3.1. Region I

239

240

241

242

243

244

For long periods, the measured CHF values do not depend on the power escalation period, and increase with subcooling. For a given Reynolds number, subcooling reduces the thickness of the superheated liquid layer, which has important implications for the bubble growth process and the overall boiling dynamics. Bubbles growing through a highly subcooled boundary layer undergo a rapid re-condensation that limits their growth. Their size decreases with increasing subcooling, as shown in Figure 6, and so does their thermal footprint. Clearly, a small bubble removes less energy than a big bubble. However, the number of bubbles that a surface can accommodate is also affected by subcooling. At low subcooling, when a bubble nucleates, it grows large and removes

energy from a large area around its nucleation site. That prevents potentially other active cavities from nucleating. At high subcooling, as bubbles are much smaller, the distance between two active nucleation sites decreases. Thus, as clearly shown in Figure 6, the nucleation site density increases.

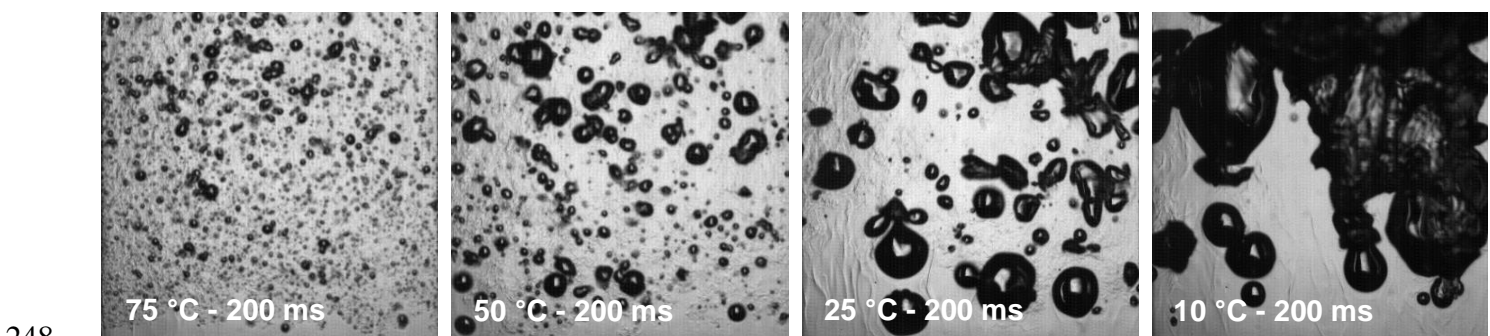


Figure 6. Visualization of the boiling process for 75, 50, 25 and 10 °C of subcooling (left to right), a Reynolds number of 35000, and a period of 200 ms. All the images correspond to an area of 1x1 cm².

For low subcooling (e.g., $\Delta T_{\text{sub}} \leq 25$ °C), the coalescence of multiple large bubbles leads to the creation of large vapor clots that separate the boiling surface from the bulk flow (see Figure 7). However, heat flux measurements show that a dominant fraction of the boiling surface under the vapor clot is still wet, suggesting the presence of a liquid layer between the surface and the vapor clot itself. Such observation seems to agree with the modeling assumptions in Refs. [16–19, 24]. However, we did not observe any stable vapor stems feeding the vapor clot. Instead, we observed bubbles nucleating and detaching from the heated surface, and coalescing with the clot.

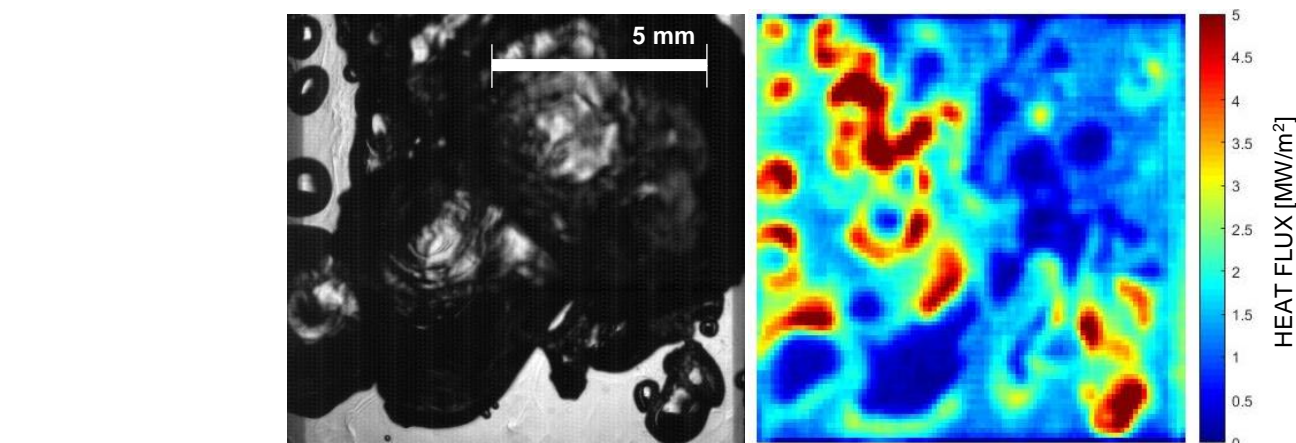
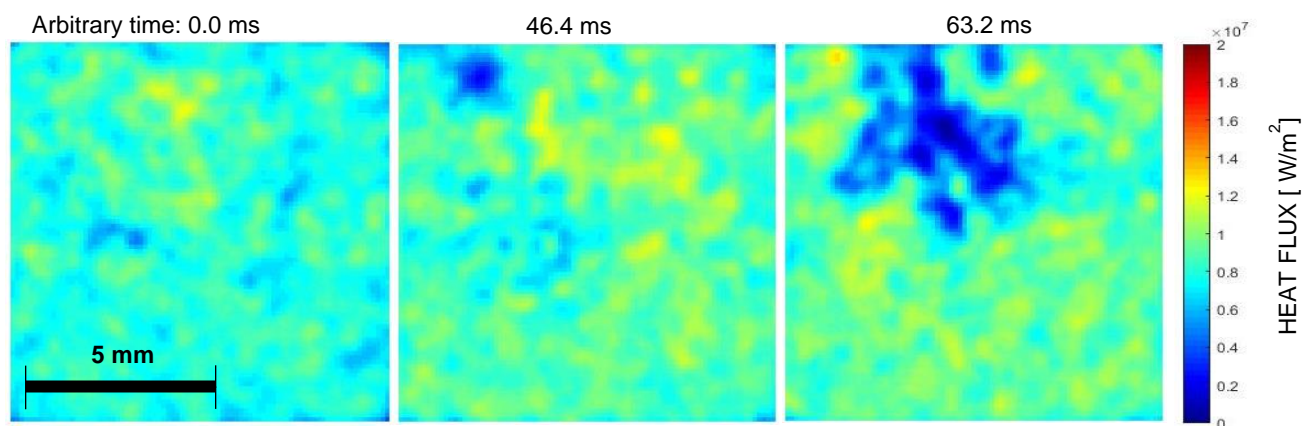


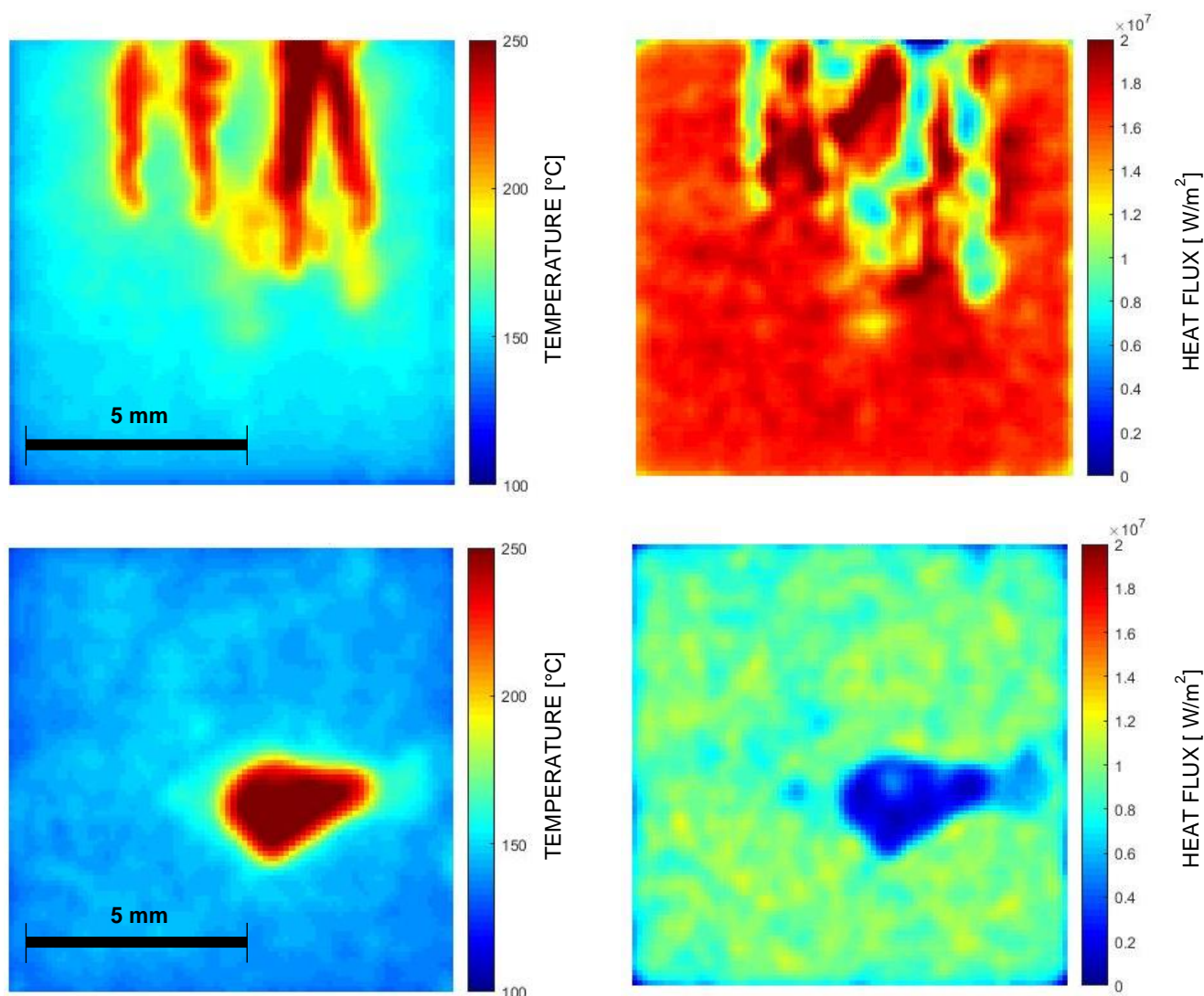
Figure 7. Simultaneous HSV image (left) and heat flux (right) on the boiling surface near CHF (precisely, at 1.84 MW/m²) at 10 °C subcooling, 35000 Reynolds number and 100 ms period. While almost the entire boiling surface is hidden behind a vapor clot, only a small fraction of it is actually dry, as shown on the right. Dry spots correspond to the surface regions where the heat flux is practically zero.

At high subcooling, bubbles are much smaller. The fluid flows throughout the length of the heater in a short time compared to the power escalation period, and it warms up as it moves upward. The temperature of both the heater and the fluid increase as the fluid moves upward. That increases bubble nucleation and reduces vapor re-condensation. Accordingly, the boiling crisis starts on the top part of the heater (see Figure 8). Interestingly, for high subcooling, the presence of flow makes the eventual dry spots to be shaped as elongated patches, aligned with the flow direction (Figure 9, top). The distance between such patches as well as the width of each patch is close to 1 mm. Such behavior could be related to the flow structure of the turbulent boundary layer. However, further investigation would be required to confirm this hypothesis. In the absence of flow, instead, the dry spots appear randomly on the heated surface, and grow with a more circular shape (Figure 9 bottom). This observation suggests that even in the presence

270 of natural circulation patterns that may appear at high subcooling and for long power escalation periods, the time scales associated
 271 with the boiling process (e.g., growth and wait time) are shorter than the time scales associated with the natural convection.
 272



273 **Figure 8.** Progression of CHF for a slow power transient with a power escalation period of 500 ms. The subcooling is 50 °C and
 274 the Reynolds number is 25000 (the fluid flows upwards). Note that the dry spots form on the top of the heater.
 275



276 **Figure 9.** Dry spot shape for a Reynolds number of 35000 (top figures) and a stagnant flow (bottom figures). The subcooling is 75
 277 °C and the power escalation period is 200 ms. The maximum temperature under the dry spot reaches values higher than 250 °C.
 278 However, the color bar is limited to 250 °C to better illustrate the contours of the dry spot.
 279

In summary, for long periods, the CHF increases almost linearly with subcooling (see Figure 10, left), as expected from the classical CHF tests done with steady heating, e.g., Ivey and Morris' database [28]. CHF also increases, but less-than-linearly, with the mass flux, G (see Figure 10, right). Here, the dependence of CHF on G is between $G^{0.2}$ and $G^{0.3}$, which is quite close to what predicted by empirical correlations for steady-state flow boiling CHF in long, uniformly heated tubes, e.g., the Tong correlation [29], for which the CHF is proportional to $G^{0.4}$.

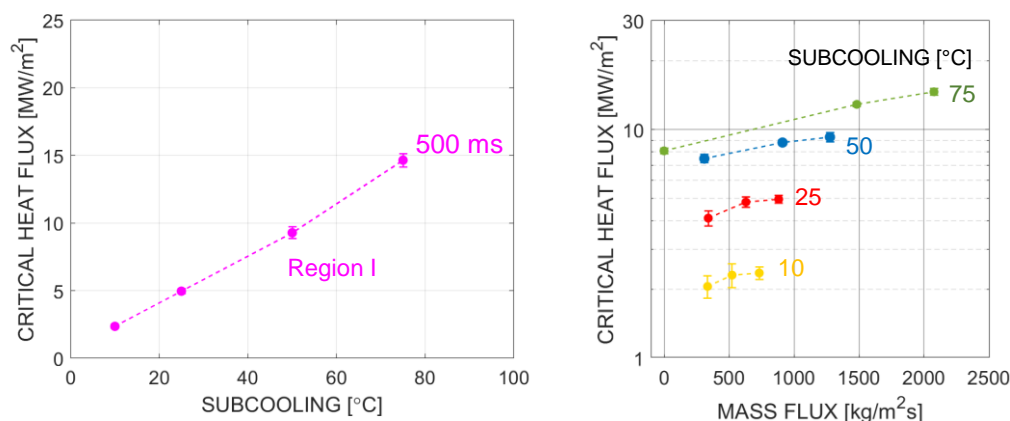


Figure 10. Effect of subcooling (Left) on CHF values for a Reynolds number of 35000 and a power escalation period of 500 ms. Effect of mass flux (Right) on CHF for different subcooling degrees and a power escalation period of 500 ms.

3.2. Region II

For high subcooling and short periods, bubbles nucleate and condense very quickly, possibly without even detaching from the heated surface. The shorter is the period, the less the flow contribute to the heat removal process. For very short periods, when the thermal transient is very fast, the distance covered by the near wall fluid throughout the duration of the transient is negligible compared to the heater length. The time scales of forced convection are also small compared to the bubble life cycle, which is in the order of 0.1 ms. In other words, the flow is “frozen.” It does not play any significant mechanical (e.g., to detach bubbles) or thermal (e.g., to remove energy form the thermal boundary layer) role. As clearly shown in Figure 11, the CHF values for very short periods, e.g., below 5 ms, do not depend on the Reynolds number, and coincide with the values obtained in stagnant water (see the right figure for 75 °C of subcooling). The CHF values in this region decrease as $1/\sqrt{\tau}$. This is the same trend observed for the asymptotic transient conduction heat removal in pool boiling [20]. This finding supports the idea that, if the flow is not strong enough, the dominant heat transfer mechanism is transient conduction. The transition between a regime dominated by forced convection effects (i.e., Region I) and a regime dominated by transient conduction heat transfer (i.e., Region II) depends on the effectiveness of the single phase forced convection, i.e., it depends on flow rate and subcooling. The period at which this transition occurs decreases with increasing Reynolds number and subcooling, as expected (see Figure 11).

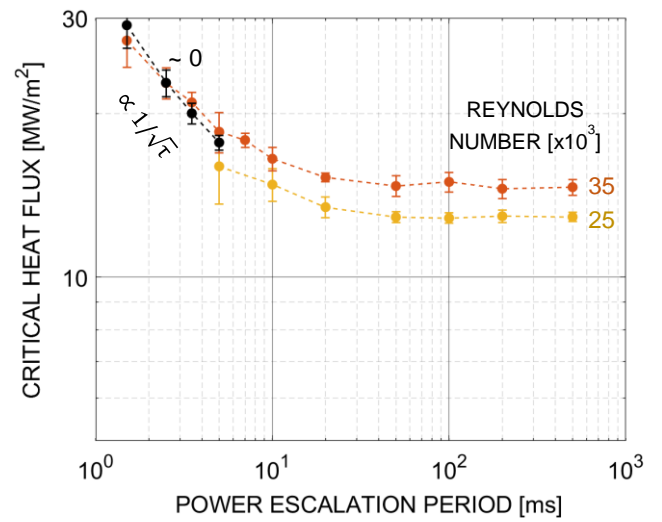
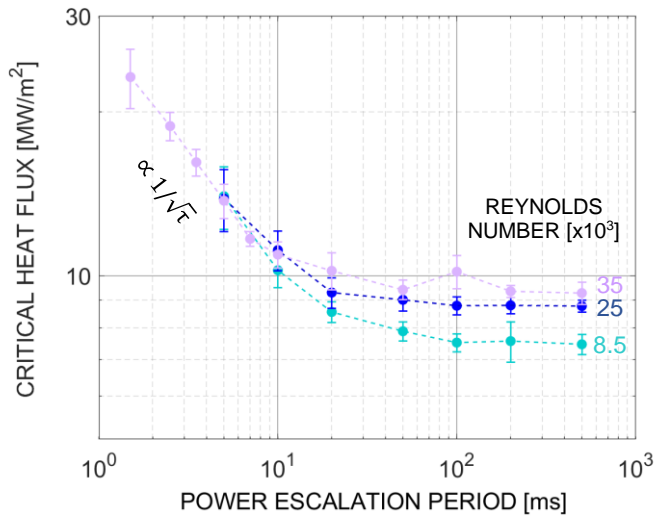


Figure 11. CHF value vs. power escalation period for 50 °C and 75 °C of subcooling at different mass fluxes.

3.3. Region IV

For low subcooling ($\Delta T_{\text{sub}} < 25$ °C) and short periods ($\tau < 10$ ms), the onset of nucleate boiling (ONB) and the boiling crisis are almost coincidental. At these operating conditions, bubbles are growing fast and coalesce immediately with each other, obstructing the liquid supply to the boiling surface (see Figure 12). Therefore, the first generation of bubbles forms irreversible dry spots as soon as their microlayers are fully evaporated. In other words, the heat flux at ONB and the CHF are very close, and only differ due to the time lag between the nucleation and the complete growth (including microlayer evaporation) of the bubble footprint on the heated surface. The temperature excursion associated with the CHF is delayed by the time required to evaporate the microlayer and any liquid trapped between the coalesced bubbles. Importantly, the onset of nucleate boiling heat flux decreases as $1/\sqrt{\tau}$ [20]. This is not surprising, as ONB conditions are also dictated by transient conduction heat transfer, as explained in Ref. [20].

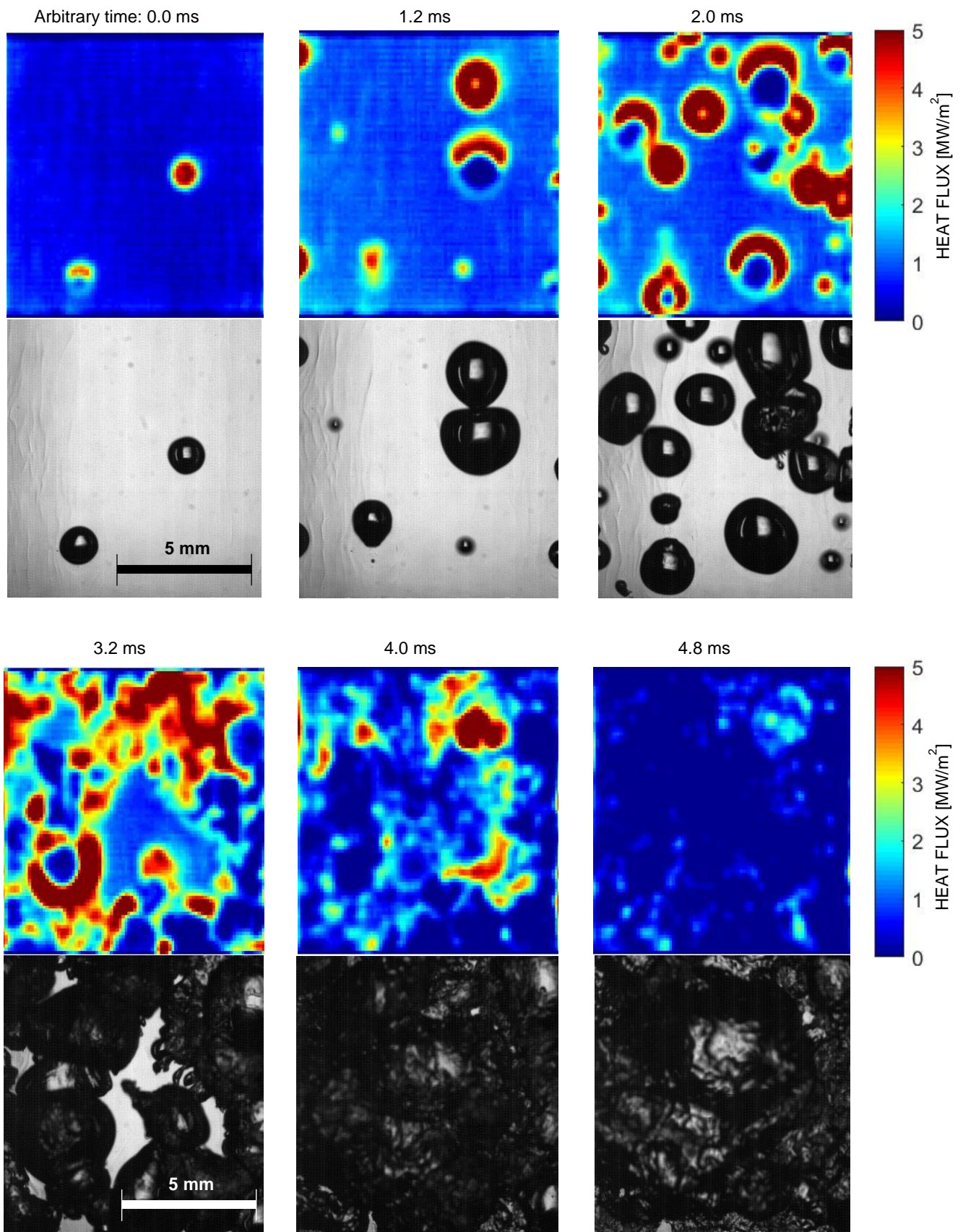


Figure 12. Progression of CHF at 10 °C subcooling, 35000 Reynolds number and 5 ms period.

3.4. Transition between region II and IV

We have observed that the CHF values decrease as $1/\sqrt{\tau}$ for both high and low subcooling. However, this same trend results from different physical mechanisms. We have seen that, for Region II (short period, high subcooling) the flow has little or no effect on the bubble dynamics and the CHF for a Reynolds number of 35000 is essentially the same as in stagnant water. The dominant heat removal mechanism is transient conduction. The cooling provided by transient conduction is strong enough for several generations of bubbles to re-condense before they merge and trigger the boiling crisis. Conversely, for very low subcooling, the first generation of bubbles grows large, and the cooling provided by transient conduction is not fast enough to make the vapor re-condense. Under this scenario the first generation of bubbles merge together and trigger the boiling crisis. The transition between Region II and IV is captured in Figure 13. Note that for both high and low subcooling the CHF is essentially linearly dependent on subcooling. This is expected for processes driven by transient conduction (i.e., in Region II) but also in Region IV, as the onset of nucleate boiling heat flux (on the same exact surface) is also linearly proportional to subcooling [20]. Thus, the transition between Region IV and II is associated with the size and the re-condensation of the vapor bubbles on the heated surface. Small bubbles in a highly subcooled liquid can easily re-condense, whereas large bubbles in slightly subcooled water do not. Importantly, Sakurai [30] hypothesized that the CHF in Region IV is caused by the heterogeneous spontaneous nucleation (HSN) in originally flooded cavities. However, HSN requires abnormally high wall superheat to occur. In our work, whatever the subcooling, ONB always occurs at relatively low superheat, consistent with the Hsu criterion [20], i.e., nucleation on cavities containing a vapor embryo.

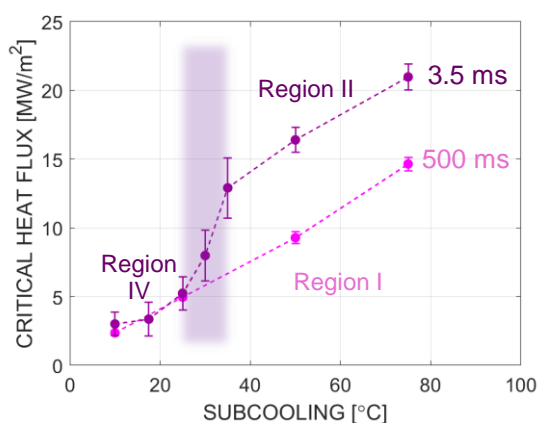


Figure 13. Effect of subcooling on CHF for a Reynolds number of 35000.

3.5. Region III and transition between region III and IV

Region III has a phenomenology similar to the one observed for Region I for low subcooling degrees and pictured in Figure 7: bubbles nucleate, grow large, and merge with the vapor clot hovering over the heated surface. Under these conditions, CHF seems to occur when the liquid layer between the vapor clot and the heated surface is fully evaporated before the vapor clot is removed by the flow. As discussed in the introduction, Serizawa [15] and later Pasamehmetoglu [15,16] adapted this description to transient heat inputs and found that CHF would increase when the period decreases. However, the transition between Region III and IV is very intriguing. At low subcooling the bubble re-condensation is weak. Thus, bubbles primarily disappear from the heated surface when they are detached by the flow. For long periods, the flow drags the bubbles away. However, for short periods, the growth and coalesce are much more rapid, and the bubbles coalesce with each other shortly after they nucleate, before the flow can push them away from the heated surface. Thus, we may expect that the transition between Region III and IV depends on the flow velocity. This behavior is investigated in Figure 14, where we compare the CHF values for power escalation periods of 5 ms, at different subcooling and for different mass fluxes. For 10, 50 and 75 °C the CHF values are rather independent of the mass flux. Precisely, the tests at 10 °C belong to Region IV, whereas the tests at 50 °C belong to Region II. Interestingly, for the highest subcooling, i.e., 75 °C, the CHF values tend to increase for the highest mass fluxes. That indicates a transition between Regions II

and I. However, the most intriguing behavior is observed for the tests run at 25 °C of subcooling. We observed that, in the region at the transition between Regions III and IV, the boiling crisis can randomly switch between Regions III and IV, even for the same mass flux. Thus, the CHF values at 25 °C of subcooling can be divided into two groups. When the boiling crisis happens after the first generation of bubbles, the CHF is lower (Region IV). By contrast, if the bubbles depart from the surface, the CHF values tend to be higher and consistent with the values expected for Regions III and I. Importantly, the difference between the CHF values decreases with the mass flux, and disappear if the flow is strong enough (here, at 1750 kg/m²/s) to consistently remove the first generation of bubbles from the heated surface.

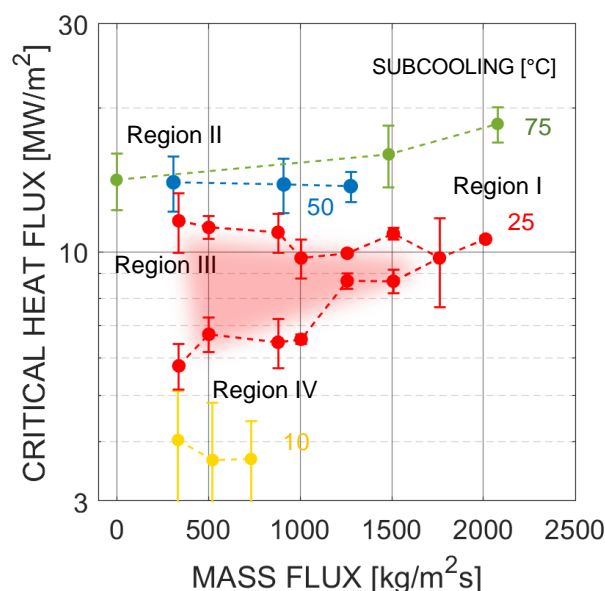


Figure 14. Effect of mass flux on CHF for different subcooling degrees at 5 ms.

In summary, the transition between Regions III and IV has a rather aleatory boundary. Increasing the mass flux is always beneficial, as the flow removes bubbles from the surface, and the higher is the flow rate, the stronger are the forces that push the bubbles away from the surface. This clarification may explain the rather scattered data from the literature (e.g., see Fig. 43 in Ref. [11]) at the transition between very short and very long power escalation periods, even for pool boiling conditions, when bubbles detach from the surface thanks to the buoyancy force.

In summary, Figure 15 is a re-plot of Figure 5, where we summarize the phenomenology, as well as the mechanisms that lead to the transition between the different Regions. **Note that, while we directly observed the chaotic transition between Regions III and IV for this specific combination of power escalation period and subcooling, i.e., 25 °C of subcooling and 5 ms of period, we expect that the period at which this transition occur may depend on the subcooling degree. While for high subcooling this is never the case, for 10 °C of subcooling this transition seems to occur between 10 and 20 ms.**

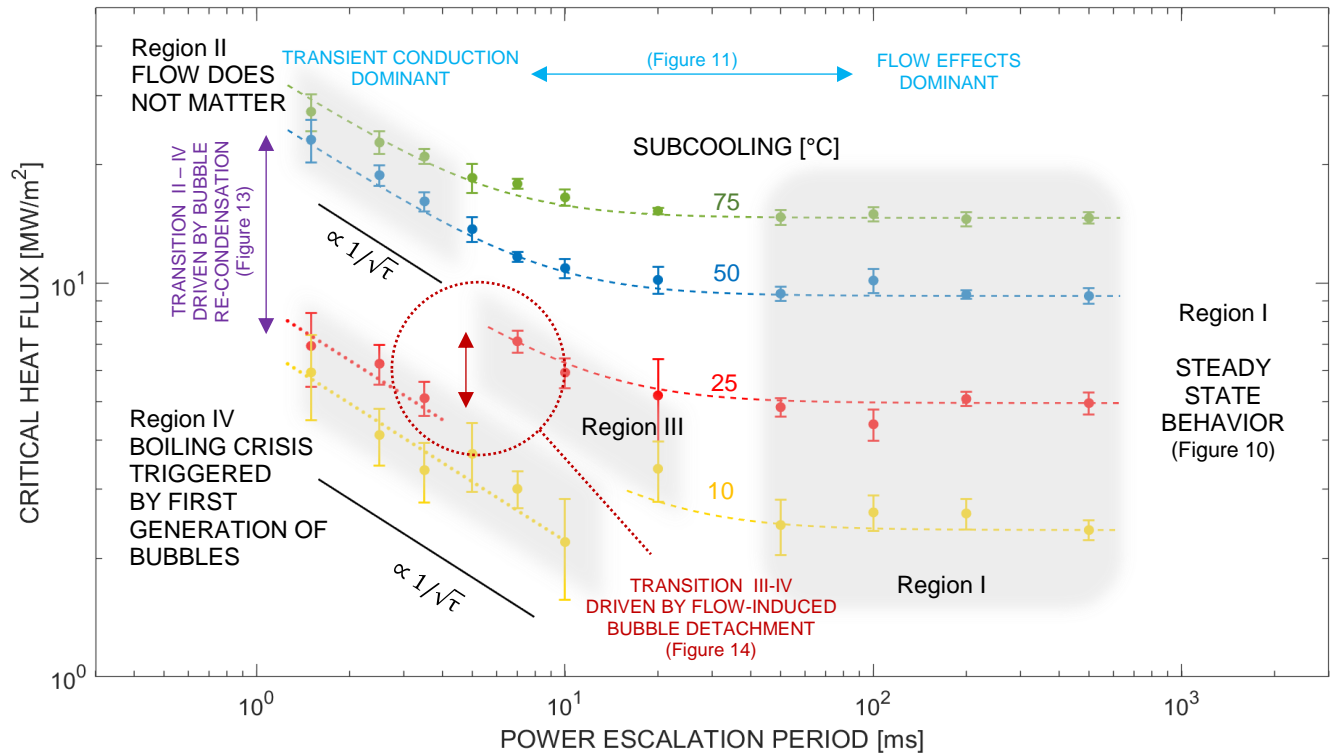


Figure 15. CHF values vs. power escalation periods for tests run with a Reynolds number of 35000, at different subcooling degrees, with a summary of the boiling phenomenology Regions, as well as the transition mechanisms.

4. Conclusions

We clarified the physical mechanisms triggering the boiling crisis of water in subcooled flow boiling under exponentially escalating heat inputs, and quantified the corresponding CHF values. We tested various values of flow velocity, water subcooling and exponential power escalation periods, τ , from 1.5 to 500 ms. For long periods, CHF is independent of the power escalation period and the transient boiling process is similar to steady state. For both low and high subcooling, the CHF values at very short periods follows an asymptotic $1/\sqrt{\tau}$ trend. However, for high subcooling the boiling crisis occurs through a fully-developed nucleate boiling process, which for short periods is dominated by transient conduction effects, and the CHF values are significantly higher than in steady-state conditions. The modeling of this transient, highly subcooled flow boiling regime will be our future focus. Also, we have clarified that, for low subcooling, the boiling crisis happens during the growth of the first generation of bubbles, which never detach from the heated surface and coalesce with each other shortly after the onset of nucleate boiling (ONB). Importantly, this explains the non-monotonic trend of the CHF values as the power escalation period is decreased for low subcooling. However, this behavior can be avoided by increasing the flow rate, which helps detaching bubbles from the surface before they can coalesce.

Acknowledgements

We thank G.Y. Su and M.C. Duluc for many insightful comments on our work. This research project was sponsored by CEA (MIT award number 025597-00001 – CEA award number DEN4193).

CRediT Authorship statement

Artyom Kossolapov: Conceptualization, Methodology, Validation, Formal Analysis, Investigation, Writing and Visualization. **Florian Chavagnat:** Methodology, Validation, Formal Analysis, Investigation, Writing – Review and Editing. **Raksmey Nop:** Validation, Formal Analysis, Writing – Review and Editing. **Nicolas Dorville:** Writing – Review and Editing, Supervision and Project Administration, Funding Acquisition. **Bren Phillips:** Investigation, Writing – Review and Editing, Supervision and Project Administration. **Jacopo Buongiorno:** Writing – Review and Editing, Supervision and Project Administration, Funding

392 Acquisition. **Matteo Bucci:** Conceptualization, Methodology, Formal Analysis, Writing and Visualization, Supervision and
393 Project Administration, Funding Acquisition.

394 **References**

- 395 [1] J. R. Dietrich and D. C. Layman, "Transient and Steady State Characteristics of a Boiling Reactor. The BORAX
396 Experiments," Lemont, 1954.
- 397 [2] J. Dugone, "SPERT III Reactor Facility: E-Core Revision," 1965.
- 398 [3] J. G. Crocker and L. A. Sephan, "Reactor Power Excursion Tests in the SPERT IV Facility," 1964.
- 399 [4] M. Ishikawa and T. Inabe, "THE NUCLEAR SAFETY RESEARCH REACTOR (NSRR) IN JAPAN."
- 400 [5] J. Papin, M. Balourdet, F. Lemoine, F. Lamare, J. M. Frizonnet, and F. Schmitz, "French Studies on High-Burnup Fuel
401 Transient Behavior Under RIA Conditions," *Nucl. Saf.*, vol. 37, pp. 289–327, 1996.
- 402 [6] V. Bessiron, "Modelling of clad-to-coolant heat transfer for RIA applications," *J. Nucl. Sci. Technol.*, vol. 44, no. 2, pp.
403 211–221, 2007.
- 404 [7] H. Takiguchi, M. Furuya, T. Arai, and K. Shirakawa, "Transient boiling flow in 5×5 rod bundle under non-uniform
405 rapid heating," *Nucl. Eng. Des.*, vol. 340, pp. 447–456, Dec. 2018.
- 406 [8] R. Visentini, C. Colin, and P. Ruyer, "Experimental investigation of heat transfer in transient boiling," *Exp. Therm. Fluid
407 Sci.*, 2014.
- 408 [9] H. Auracher and W. Marquardt, "Experimental studies of boiling mechanisms in all boiling regimes under steady-state
409 and transient conditions," *Int. J. Therm. Sci.*, vol. 41, no. 7, pp. 586–598, Jun. 2002.
- 410 [10] M. W. Rosenthal and R. L. Miller, "An experimental study of transient boiling," Oak Ridge, Tennessee, 1957.
- 411 [11] A. Sakurai, "Mechanisms of transitions to film boiling at CHF in subcooled and pressurized liquids due to steady and
412 increasing heat inputs", *Nucl. Eng. Des.*, vol. 197, no. 3. 2000.
- 413 [12] H. A. Johnson, "Transient boiling heat transfer to water," *Int. J. Heat Mass Transf.*, vol. 14, no. 1, pp. 67–82, 1971.
- 414 [13] I. Kataoka, A. Serizawa, and A. Sakurai, "Transient boiling heat transfer under forced convection," *Int. J. Heat Mass
415 Transf.*, vol. 26, no. 4, pp. 583–595, 1983.
- 416 [14] A. Sakurai and M. Shiotsu, "Transient Pool Boiling Heat Transfer Part 2: Boiling Heat Transfer and Burnout," *J. Heat
417 Transfer*, vol. 99, pp. 547–553, 1977.
- 418 [15] J. Park, K. Fukuda, and Q. Liu, "Transient CHF Phenomena Due to Exponentially Increasing Heat Inputs," *Nucl. Eng.
419 Technol.*, vol. 41, no. 9, pp. 1206–1214, 2009.
- 420 [16] A. Serizawa, "Theoretical prediction of maximum heat flux in power transients," *Int. J. Heat Mass Transf.*, 1983.
- 421 [17] Y. Haramura and Y. Katto, "A new hydrodynamic model of critical heat flux, applicable widely to both pool and forced
422 convection boiling on submerged bodies in saturated liquids," *Int. J. Heat Mass Transf.*, vol. 26, no. 3, pp. 389–399, Mar.
423 1983.
- 424 [18] K. O. Pasamehmetoglu, R. A. Nelson, and F. S. Gunnerson, "Critical Heat Flux Modeling in Pool Boiling for Steady-
425 State and Power Transients," *J. Heat Transfer*, vol. 112, no. 4, p. 1048, Nov. 1990.
- 426 [19] K. O. Pasamehmetoglu, R. A. Nelson, and F. S. Gunnerson, "Critical Heat Flux modeling in Forced Convection Boiling
427 During Power Transients," *J. Heat Transfer*, vol. 112, pp. 1058–1062, 1990.
- 428 [20] G.-Y. Su, M. Bucci, T. McKrell, and J. Buongiorno, "Transient boiling of water under exponentially escalating heat
429 inputs. Part I: Pool boiling," *Int. J. Heat Mass Transf.*, vol. 96, pp. 667–684, 2016.
- 430 [21] G. Y. Su, M. Bucci, T. McKrell, and J. Buongiorno, "Transient boiling of water under exponentially escalating heat
431 inputs. Part II: Flow boiling," *Int. J. Heat Mass Transf.*, vol. 96, pp. 685–698, 2016.
- 432 [22] A. Richenderfer *et al.*, "Investigation of subcooled flow boiling and CHF using high-resolution diagnostics," *Exp. Therm.
433 Fluid Sci.*, 2018.
- 434 [23] M. Bucci, A. Richenderfer, G. Y. Su, T. McKrell, and J. Buongiorno, "A mechanistic IR calibration technique for boiling
435 heat transfer investigations," *Int. J. Multiph. Flow*, vol. 83, pp. 115–127, 2016.
- 436 [24] M. Ravichandran and M. Bucci, "Online, quasi-real-time analysis of high-resolution, infrared, boiling heat transfer
437 investigations using artificial neural networks," *Appl. Therm. Eng.*, vol. 163, p. 114357, Dec. 2019.
- 438 [25] L. Zhang, J. H. Seong, and M. Bucci, "Percolative Scale-Free Behavior in the Boiling Crisis," *Phys. Rev. Lett.*, vol. 122,
439 no. 13, Apr. 2019.
- 440 [26] G. Y. Su *et al.*, "On the oscillatory nature of heat transfer in steady annular flow," *Int. Commun. Heat Mass Transf.*, vol.
441 108, no. September, p. 104328, 2019.
- 442 [27] J.-M. Le Corre, S.-C. Yao, and C. H. Amon, "Two-phase flow regimes and mechanisms of critical heat flux under
443 subcooled flow boiling conditions," *Nucl. Eng. Des.*, vol. 240, no. 2, pp. 245–251, 2010.
- 444 [28] H. J. Ivey and D. J. Morris, "Critical Heat Flux of Saturated and Subcooled Pool Boiling in Water at Atmospheric
445 Pressure," in *International Heat Transfer Conference*, 1966, pp. 129–142.
- 446 [29] N. E. Todreas and M. S. Kazimi, *Nuclear Systems Volume I: Thermal-Hydraulics Fundamentals*. CRC Press, 2011.
- 447 [30] A. Sakurai, M. Shiotsu, K. Hata, and K. Fukuda, "Photographic study on transitions from non-boiling and nucleate
448 boiling regime to film boiling due to increasing heat inputs in liquid nitrogen and water," *Nucl. Eng. Des.*, vol. 200, no.
449 1–2, pp. 39–54, Aug. 2000.
- 450